Hindawi
Geofluids
Volume 2019, Article ID 6074892, 11 pages
https://doi.org/10.1155/2019/6074892

Research Article

Dynamic Characteristics of Offshore Natural Gas Hydrate Dissociation by Depressurization in Marine Sediments

Xinfu Liu,[1,2] **Chunhua Liu**,[3] **and Jianjun Wu**[4]

[1]*School of Mechanical and Automotive Engineering, Qingdao University of Technology, Qingdao, Shandong 266520, China*
[2]*Key Lab of Industrial Fluid Energy Conservation and Pollution Control, Ministry of Education, Qingdao, 266520 Shandong, China*
[3]*College of Mechanical and Electronic Engineering, China University of Petroleum (East China), Qingdao, Shandong 266580, China*
[4]*PetroChina Coalbed Methane Co., Ltd., Xian, Shanxi 710082, China*

Correspondence should be addressed to Xinfu Liu; upcdoctor@126.com and Chunhua Liu; 20090053@upc.edu.cn

Received 10 April 2019; Revised 10 August 2019; Accepted 5 September 2019; Published 13 November 2019

Academic Editor: Umberta Tinivella

Dynamic characteristics of offshore natural gas hydrate (NGH) dissociation will provide the theoretical basis to analyze technical issues of oceanic hydrate exploitation. A mathematical model is developed to simulate offshore NGH dissociation by depressurization in marine sediments. Different phase combination statuses are involved in the process of NGH dissociation by taking ice melting and water freezing into account. The proposed methodology can analyze the processes of hydrate and water phase transitions, decomposition kinetics and thermodynamics, viscosity and permeability, ice-water phase equilibrium, and natural gas and water production. A set of an experimental system is built and consists of one 3-D visual reactor vessel, one isothermal seawater vessel, one natural gas and water separator, and one data acquisition unit. The experiments on offshore NGH dissociation by depressurization in 3-D marine sediments are carried out, and this methodology is validated against the full-scale experimental data measured. The results show that during the prophase, natural gas flow is preceded by water flow into the production wellbore and natural gas occupies more continuous flow channels than water under a large pressure gradient. Then, the natural gas flow rate begins to decline accompanied by an increase of water production. During the second phase, natural gas flow rate decreases slowly because of the decreased temperature of hydrate-bearing formation and low pressure gradient. The lower the intrinsic permeability in marine sediments, the later the water flow rate reaches the peak production. And the space interval of the production wellbore should be enlarged by an increase of the intrinsic permeability. The stable period of natural gas production enhances, and the water flow rate reduces with the increase of bottom-hole pressure in production wellbores. The main reason is the slow offshore NGH dissociation under the low producing pressure and the restriction of heat conductivity under the low temperature.

1. Introduction

Natural gas hydrates (NGHs) are ice-like crystalline compounds in which hydrocarbon gas molecules are encaged inside voids in interlocking bucky-ball-type cage structures of water molecules under suitable conditions of high pressure and low temperature. NGH sequesters hydrocarbon natural gases while the gas hydrate extracts dissolved natural gas from pore water [1, 2]. The reactions of dissolution and growth are highly reversible for NGH. Bonding of gas molecules in the cage of water molecules is accomplished by van der Waals force [3, 4].

Analysis on dissociation of offshore NGH will provide the theoretical basis to analyze technical issues of oceanic hydrate exploitation. There have been the basic researches on dynamic characteristics of NGH dissociation [5, 6]. Selim and Sloan [7] described gas hydrate dissociation under thermal stimulation in porous media. The proposed model viewed gas hydrate dissociation as a process of natural gas and water produced at a moving boundary. However, the proposed models were somewhat simple because of the limitation of NGH in marine sediments at that time. Clarke and Bishnoi [8–10] determined the intrinsic rate constants and activation energies for the dissociation of different

NGHs. The proposed models neglected heat transfer and mass transfer because of the high stirring rate. He et al. [11] regarded gas hydrate decomposition as a gas-solid reaction without solid production layer with the temperature of above zero centigrade. The particle shrinking problem of NGH decomposition was studied from the crystal dissolution angle. In recent years, the models of depressurization dissociation described the effects of pressure drop, ΔP, on NGH dissociation by depressurization at some constant temperature. And the dissociation process in hydrate-bearing porous media was developed from Stefan's equations [12–14] to the models combining multiphase flows and intrinsic kinetic process of NGH [15]. The basic researches mainly studied the effects of the driving drop of temperature ΔT and pressure ΔP on dissociation. This establishes the dissociation kinetic process of NGH. Ruffine et al. [16–20] focused on hydrate reservoir exploration and field production tests using different porous media or sediment systems. Boxall et al. [21–23] reported on the mechanism of hydrate dissociation in stirring reactors. The hydrate dissociation rate can be enhanced by increasing the experimental temperature or decreasing the experimental pressure. Meanwhile, the agglomeration of wetted hydrate particles in the initial hydrate dissociation stage was observed in detail by FBRM and PVM data.

The applied researches mainly involved studies on dynamics of NGH dissociation. And they were directed toward the dynamic simulation of hydrate dissociation in pipelines and real hydrate dissociation in porous media [24–26]. Sun and Mohanty [27] developed a simulator for methane hydrate formation and dissociation in porous media with the system of gas and ice consideration. And the simulation of intrinsic kinetics was carried out based on the Kim-Bishnoi model. However, no experimental results were found in their works. Liang et al. [28] and Kumar et al. [29] developed a mathematical model to describe the kinetics of methane hydrate dissociation below the ice point based on an ice-shielding mechanism. Tang et al. [30] carried out the experimental works of 1-D gas production from the hydrate-bearing core by depressurization with the simulator TOUGH-Fx/Hydrate. However, the effect of hydrate dissociation kinetics and the ice phase were neglected in their works. Nazridoust and Ahmadi [31] developed Users' Defined Subroutines (UDS) using the FLUENT™ code. And an axisymmetric model of the core was solved for multiphase gas-liquid flows during the hydrate dissociation process. The axisymmetric model contained three separate phases: methane gas, water, and methane hydrate. However, their works assumed that gas hydrate was dispersed in the pores of the core. Kneafsey and Moridis [32] observed the changes of internal temperature and density during methane hydrate dissociation by depressurization in a Mount Elbert sandstone sample. However, the experimental results include only hydrate dissociation having occurred initially throughout the sample with the temperature maintained above the ice point. Windmeier et al. [33–35] recognized that mass transfer was the dominant factor near the dispersed hydrate-liquid interface during hydrate dissociation and developed the Consecutive Desorption and Melting (CDM) model. Chen et al. [36] and Shi et al. [37] developed an improved hydrate dissociation model by considering the changes in the dissociated surface induced by particle agglomeration. Therefore, it is necessary to further improve the model of dissociation under depressurization conditions, especially for offshore NGH in marine sediments, by considering heat transfer, mass transfer, and intrinsic kinetics.

The proposed dissociation model contains multiphase flows: gas, water, hydrate, and ice. Different phase combination statuses are involved in the process of NGH dissociation by taking ice melting and water freezing into account. This methodology can analyze the processes of hydrate and water phase transitions, decomposition kinetics and thermodynamics, viscosity and permeability, ice-water phase equilibrium, and natural gas and water production. A set of an experimental system is built, and some experiments on offshore NGH dissociation by depressurization in 3-D marine sediments are carried out.

2. Model Development of Offshore NGH Dissociation by Depressurization

In terms of characteristics and behavior, offshore NGHs are crystalline, ice-like substances belonging to a class of compounds called clathrates. The chemical compounds have natural-gas molecules bound within almost spherical water cages through physical rather than chemical bonds. The offshore NGH dissociation simulator contains three components (NGH, natural gas, and water) and four separate phases (gas, water, hydrate, and ice). Processes of hydrate and water phase transitions, decomposition kinetics, and thermodynamics are considered in the NGH dissociation simulator. And then a three-dimensional (3-D) hydrate-bearing marine sediment is developed based on the conservation of mass and energy [38–40].

Furthermore, some assumptions are made as follows: (1) Darcy's law is valid for a two-phase (gas and water) flow; (2) the water phase contains only free water, and the ice phase contains only the component of water; (3) the effect of salt concentration on synthesis and decomposition of the hydrate is neglected; (4) the molecular diffusion and hydrodynamic dispersion are neglected in mass transportation. Therefore, the equations of mass balance for the phases of gas, water, ice, and NGH can be, respectively, given by

$$\frac{\partial}{\partial t}\left(\phi\rho_{\mathrm{ng}}S_{\mathrm{ng}}\right) = \nabla\left[\nabla\left(p_{\mathrm{ng}} + \rho_{\mathrm{ng}}g\Delta Z\right)\frac{\rho_{\mathrm{ng}}k_{\mathrm{ng}}}{\mu_{\mathrm{ng}}}\right] + q_{\mathrm{ng}} + \bar{m}_{\mathrm{ng}}, \tag{1}$$

$$\frac{\partial}{\partial t}\left(\phi\rho_{\mathrm{w}}S_{\mathrm{w}} + \phi\rho_{\mathrm{I}}S_{\mathrm{I}}\right) = \nabla\left[\nabla\left(p_{\mathrm{w}} + \rho_{\mathrm{w}}g\Delta Z\right)\frac{\rho_{\mathrm{w}}k_{\mathrm{w}}}{\mu_{\mathrm{w}}}\right] + q_{\mathrm{w}} + \bar{m}_{\mathrm{w}} + \bar{m}_{\mathrm{I}}, \tag{2}$$

$$\frac{\partial}{\partial t}\left(\phi\rho_{\mathrm{mh}}S_{\mathrm{mh}}\right) = \bar{m}_{\mathrm{mh}}. \tag{3}$$

The subscripts of I, mh, ng, and w denote the separate phases of ice, NGH, natural gas, and water, respectively. The parameters of $\bar{m}$, ρ, S, and Φ are the flow rate of

decomposition, density, saturation, and porosity, respectively. The relationship of saturation of these phases satisfies that $S_I + S_{mh} + S_{ng} + S_w = 1$, where g is the gravitational acceleration, k_{ng} and k_w are the permeabilities of natural gas and water, respectively; p_{ng} and p_w are the flowing pressures of natural gas and water, respectively; q_{ng} and q_w are the injected natural gas and water at the boundary, respectively; and μ_{ng} and μ_w are the viscosities of natural gas and water, respectively.

q_{ng} and q_w can be evaluated from the given formulae:

$$q_{ng} = 1.571 \frac{\rho_{ng} k_{ng}}{\mu_{ng}} \frac{p_{wf} - p_{ng}}{\ln(r_e/r_b)} \delta(X - X_0, Y - Y_0, Z - Z_0), \tag{4}$$

$$q_w = 1.571 \frac{\rho_w k_w}{\mu_w} \frac{p_{wf} - p_w}{\ln(r_e/r_b)} \delta(X - X_0, Y - Y_0, Z - Z_0), \tag{5}$$

where p_{wf} is the bottom-hole pressure of the production wellbore [41–44]; r_b and r_e are the radii of the wellbore and the supply boundary, respectively; $\delta(X, Y, Z)$ is the Dirac function of δ; X, Y, and Z are the coordinates of the Cartesian coordinate system; and X_0, Y_0, and Z_0 are the coordinates of the production wellbore.

The equation of the energy balance for the multiphase flows can be determined as follows:

$$\begin{aligned} \frac{\partial}{\partial t}(h_m T) = {} & \nabla\left[\nabla(p_w + \rho_w g \Delta Z) \frac{\rho_w k_w}{\mu_w} h_w T\right] \\ & + \nabla\left[\nabla\left(p_{ng} + \rho_{ng} g \Delta Z\right) \frac{\rho_{ng} k_{ng}}{\mu_{ng}} h_{pg} T\right] \\ & + \nabla(C_m \nabla T) + \bar{m}_I \Delta E_I - \bar{m}_{mh} \Delta E_{mh} + q_m + q_e, \end{aligned} \tag{6}$$

$$\begin{aligned} h_m = {} & (1 - \phi)\rho_s h_s + \phi\left(S_{mh}\rho_{mh}h_{mh} + S_{ng}\rho_{ng}h_{cg}\right. \\ & \left. + S_w\rho_w h_w + S_I\rho_I h_I\right), \end{aligned} \tag{7}$$

$$C_m = (1 - \phi)C_s + \phi\left(S_{mh}C_{mh} + S_{ng}C_{ng} + S_wC_w + S_IC_I\right), \tag{8}$$

where h_I, h_{mh}, h_{ng}, h_s, and h_w are the coefficients of effective specific heats of ice, NGH, natural gas, marine sediment, and water, respectively; h_{cg} and h_{pg} are the effective specific heats at constant volume and pressure, respectively; C_I, C_{mh}, C_{ng}, C_s, and C_w are the effective thermal conductivities of ice, NGH, natural gas, marine sediment, and water, respectively; ΔE_I and ΔE_{mh} are the enthalpy changes in ice melting and NGH dissociation, respectively; and q_e is the energy conducted through marine sediments.

q_m is the energy conducted through the bottom hole and well head and can be evaluated from the give formula:

$$\begin{aligned} q_m = {} & 1.571\delta(X - X_0, Y - Y_0, Z - Z_0) \\ & \cdot \left[\frac{\rho_{ng} k_{ng}}{\mu_{ng}} \frac{p_{wf} - p_{ng}}{\ln(r_e/r_b)} h_{cg} T + \frac{\rho_w k_w}{\mu_w} \frac{p_{wf} - p_w}{\ln(r_e/r_b)} h_w T\right]. \end{aligned} \tag{9}$$

The pressures of natural gas and water are related to the equation of capillary force:

$$p_c(S_w) = p_{ng} - p_w. \tag{10}$$

The permeabilities of natural gas and water are usually described in terms of the intrinsic permeability in marine sediments and relative permeability, as follows:

$$\begin{aligned} k_{ng} &= k(1 - S_{mh})^n k_{rng} = k(1 - S_{mh})^n f_1\left(S_{ng}, S_w\right), \\ k_w &= k(1 - S_{mh})^n k_{rw} = k(1 - S_{mh})^n f_2\left(S_{ng}, S_w\right), \end{aligned} \tag{11}$$

where k is the intrinsic permeability in marine sediments, k_{rng} and k_{rw} are the relative permeabilities of natural gas and water, respectively; and n is the exponential parameters for permeability.

By neglecting the change in porosity (porous media is almost incompressible), the storage terms of water and natural gas can be developed as follows:

$$\begin{aligned} \frac{\partial}{\partial t}(\rho_w \phi) &= \rho_w \phi C_{wc} \frac{\partial p}{\partial t}, \\ p_{ng} V &= Z \frac{m_{ng}}{M_{ng}} RT, \end{aligned} \tag{12}$$

where C_{wc} is the coefficient of compressibility of water in marine sediments [45], M_{ng} is the molar mass of natural gas, m_{ng} is the quality of natural gas, R is the universal gas constant, V is the volume of natural gas, and Z is the compressibility factor of natural gas.

The compressibility factor of natural gas, Z, illustrates the ratio of actual volume to ideal volume under the condition of identical quality. This compressibility factor is known as a function of pseudoreduced density, ρ_{pr}, and pseudoreduced temperature, T_{pr}, for the pure natural gas. An explicit factor, which is an accurate mathematical approximation [46, 47], is developed on the basis of experimental results and is given by

$$\begin{aligned} Z = {} & \frac{0.299 - 2.188 \times 10^{-2}\gamma_{ng} - 4.689 \times 10^{-3}\gamma_{ng}^2}{\rho_{pr} T_{pr}} \exp \\ & \cdot \left[-1.2\left(\frac{T_{pr} - 1}{T_{pr}}\right)^2\right], \\ T_{pr} = {} & 103.89 + 183.33\gamma_{ng} - 39.722\gamma_{ng}^2, \end{aligned} \tag{13}$$

where γ_{ng} is the specific gravity of natural gas in marine sediments.

The boundary conditions of this proposed model are given by

$$\begin{cases} p(0,0,0,t) = p_{wf}, \\ T(0,0,0,t) = T_{wf}, \\ \nabla p_{ng} \dfrac{\rho_{ng} k_{ng}}{\mu_{ng}} = 0, \\ \nabla p_{w} \dfrac{\rho_{w} k_{w}}{\mu_{w}} = 0, \end{cases} \tag{14}$$

and the initial conditions of this proposed model are given by

$$\begin{cases} p_{ng}(x,y,z,t)|_{t=0} = p_0, \\ T(x,y,z,t)|_{t=0} = T_0, \\ S_{mh}(x,y,z,t)|_{t=0} = S_{mh0}, \\ S_{w}(x,y,z,t)|_{t=0} = S_{w0}, \end{cases} \tag{15}$$

where p_0, S_{mh0}, S_{w0}, and T_0 are the initial distributions of pressure of natural gas, saturation of NGH, saturation of water, and temperature, respectively, and T_{wf} is the temperature at the bottom of the wellbore.

Dissociation kinetics of NGH is based on the Kim-Bishnoi model [48, 49]. Then, the flow rate of natural gas generated by NGH dissociation can be evaluated as follows:

$$\bar{m}_{ng} = K_0 \exp\left(-\frac{\Delta E_{hd}}{RT}\right) M_{ng} A_{hd} (F_l - F_e), \tag{16}$$

where A_{hd} is the specific surface area of NGH dissociation in marine sediments, F_e is the equilibrium fugacity of natural gas, F_l is the local fugacity of natural gas, K_0 is the kinetic dissociation constant which is equal to 1.25×10^5 mol/m$^2 \cdot$ Pa $\cdot$ s, and ΔE_{hd} is the activation energy of NGH dissociation given by $-E_{hd}/R = 9.75 \times 10^3$ K.

The flow rate of water generated by NGH dissociation can be given by

$$\bar{m}_{w} = \bar{m}_{ng} N_{mh} \frac{M_w}{M_{ng}}. \tag{17}$$

The decomposition rate of NGH dissociation can be determined as follows:

$$\bar{m}_{mh} = -\bar{m}_{ng} \frac{M_{mh}}{M_{ng}}, \tag{18}$$

where M_{mh} and M_w are the molar masses of NGH and water and N_{mh} is the hydration number and is given as 5.75 in the actual construction of NGH.

3. Computation of Variables and Numerical Solution

Some additional relationships need to be considered to close the equations of the NGH dissociation in porous marine sediments. Viscosity of natural gas is known as a function of temperature and pressure and can be evaluated with modification of the Amooey [50] model.

$$\begin{aligned} \mu_{ng} = {} & -3.78 \times 10^{-12} T^3 + 3.28 \times 10^{-9} T^2 \\ & + 2.88 \times 10^{-5} T + 2.45 \times 10^{-3} + 1.84 \times 10^{-13} \rho_{ng}^4 \\ & - 5.82 \times 10^{-10} \rho_{ng}^3 + 2.51 \times 10^{-7} \rho_{ng}^2 + 2.09 \times 10^{-5} \rho_{ng}. \end{aligned} \tag{19}$$

Relative permeabilities of natural gas and water and capillary pressure are determined with the modified Corey model [51, 52].

$$\begin{aligned} k_{rng} &= \left[\frac{1.54 S_{ng} - 0.077 (S_w + S_{ng})}{S_w + S_{ng}}\right]^2, \\ k_{rw} &= \left[\frac{1.54 S_{w} - 0.46 (S_w + S_{ng})}{S_w + S_{ng}}\right]^4, \\ p_c &= p_{ce} \left[\frac{1.43 S_{w} - 0.43 (S_w + S_{ng})}{S_w + S_{ng}}\right]^{-0.65}, \end{aligned} \tag{20}$$

where p_{ce} is the entry capillary pressure.

The equilibrium equation of NGH can be read as [53]

$$p_e = 1.15 \exp\left(49.318 - \frac{9.459 \times 10^3}{T}\right), \tag{21}$$

where p_e is the pressure of the NGH phase equilibrium.

The effect of pressure on the ice-water phase equilibrium is usually low since the magnitude of pressure in porous marine sediments varies from 10^6 Pa to 10^7 Pa [54]. Furthermore, possible phase combination statuses can be natural gas +NGH+water+ice, natural gas+NGH+water, natural gas+NGH+ice, natural gas+water+ice, NGH+water+ice, NGH+ice, natural gas+ice, NGH+water, etc. And the existence of the ice phase complicates the process of NGH dissociation.

NGH dissociation in marine sediments is an endothermic process of phase transition. The latent heat for per kilogram of NGH in the process of phase transition can be evaluated from the given formula [55, 56]:

$$\Delta H_{ep} = A_{ep} T + B_{ep}, \tag{22}$$

where A_{ep} and B_{ep} are the constants given by $A = -1.05$ J/(kg $\cdot$ K) and $B = 3.527 \times 10^6$ J/kg and ΔH_{ep} is the drop of latent heat in the process of phase transition.

Different phase combination statuses are involved in the process of NGH dissociation by taking ice melting and water freezing into account. The traditional approaches of

simulation are not the most suitable as far as NGH dissociation in marine sediments are concerned. The main reasons are that the unknowns are usually the same at different times for each grid block and the numerical solution must consider very small incremental times. Therefore, the fully implicit numerical methodology is introduced to discrete the partial differential equations and track the phase transition between the ice and water phases. The nonlinear algebraic equations are discretized and solved using the Newton-Raphson method. And the following steps for the calculation procedures are proposed for NGH dissociation.

(1) The supply boundary and phase status of each grid block are determined for the NGH dissociation system in porous media of marine sediments

(2) The boundary conditions and initial conditions are input, respectively, at time 0. And at each time step, the existence of the different phases for each grid block must be determined from the results of the previous time step

(3) The primary variables of the NGH dissociation model are chosen at the current time step and the equations related to their grid blocks determined. When the phase status of grid blocks is switched to water and ice, the corresponding equations of grid blocks include equations (1), (2), (3), (4), (5), and (6).

(4) The physical parameters of NGH are first solved explicitly, followed by explicit solution of natural gas and water. Then, the pressure of phase equilibrium, decomposition rate, relative permeability, and capillary pressure of NGH are solved implicitly, followed by the implicit solution of natural gas and water

(5) The matrix of coefficients for temperature, pressure, and saturation are built up for different separate phases

(6) The preconditioned conjugate gradient method is used to solve the system by discretizing the equations. Determine the iteration convergence conditions and update the next time step given by $t_{n+1} = t_n + \Delta t$

(7) Iterate by returning to step 3 until the target accuracy is obtained for the different variables

4. Verification of the Model and Interpretation

Performance of the mathematical model is demonstrated by comparing the numerical results of offshore NGH dissociation by depressurization with experimental results. A 3-D marine sediment is considered to clarify the dynamic process of offshore NGH dissociation. This 3-D marine sediment includes a NGH bearing zone located between an impermeable cover and bottom layers under depressurization.

The process flow diagram of offshore NGH formation and dissociation system by depressurization is given in Figure 1. This experimental system consists of one 3-D visual reactor vessel supplying the system with gas (natural gas and N_2) and fresh water, one isothermal seawater vessel, one natural gas and water separator, and one data acquisition unit. The 3-D visual reactor vessel can be operated up to 9.0 MPa and is enclosed in the isothermal seawater vessel with a seawater condition. The isothermal seawater is provided by a circulating pump at the temperature range from -10°C to 50°C. The production well is located at the corner of the 3-D visual reactor vessel. The formation of offshore NGHs and their dissociation in the case of depressurization, ice melt, and water freeze can be observed in the 3-D visual reactor vessel. Nine inlet pipes, thirty-six temperature sensors, and nine pressure sensors are evenly installed and arranged on the upper side of the 3-D visual reactor vessel in the manner of 3×3, 6×6, and 3×3, respectively. Nine inlet pipes are laid to supply high-pressure natural gas or N_2. Thirty-six temperature sensors are laid to detect the distribution variation of NGH saturation with time and space. The data acquisition unit can record all the information varying with time, which includes the spatial distributions of pressure, temperature, and saturations of natural gas, NGH, water, and ice. Then, the offshore NGH formation and dissociation in 3-D marine sediment, thermal stimulation, and inhibitor injection can be achieved with this experimental system.

The sea sands, with grain size ranging from 150 μm to 350 μm, are pushed tightly into the reactor vessel, which simulates the 3-D marine sediments. The upper outlet valves are closed, and the 3-D visual reactor vessel is saturated with fresh water with the booster pump and electric heater from the water vessel. Then, the natural gas is injected slowly up to a pressure higher than the pressure of the NGH phase equilibrium. At the same time, the isothermal seawater circulates in a vessel by a circulating pump. The 3-D visual reactor vessel is kept at a constant temperature environment for over 48 h. Then, the temperature of isothermal seawater is decreased down to the working temperature. Furthermore, the pressure is reduced in the 3-D visual reactor vessel and then maintains at a constant value. The formation process of NGH lasts for more than 3 days in the case of marine sediments. Finally, the backpressure in the 3-D visual reactor vessel is decreased down to a value lower than the equilibrium pressure of NGH. Natural gas and water dissociate. The resulting natural gas flow rate is recorded by flow element of the rotameter, and the resulting water flow rate is recorded by turbine flowmeter. Data of pressure and temperature are monitored during NGH dissociation by one transmitter and recorded in the data acquisition unit. The experimental results show that with the depletion of pressure in the hydrate-bearing formation, NGH dissociates, temperature falls, saturations of natural gas and water rise, and ice appears in the formation near the production well.

To clarify the dynamic process of offshore NGH dissociation in a field scale, the main experimental parameters and independent variables are presented in Table 1. These independent variables are given in order to illustrate the computation of the design objective function for the offshore NGH dissociation system by depressurization in marine sediments.

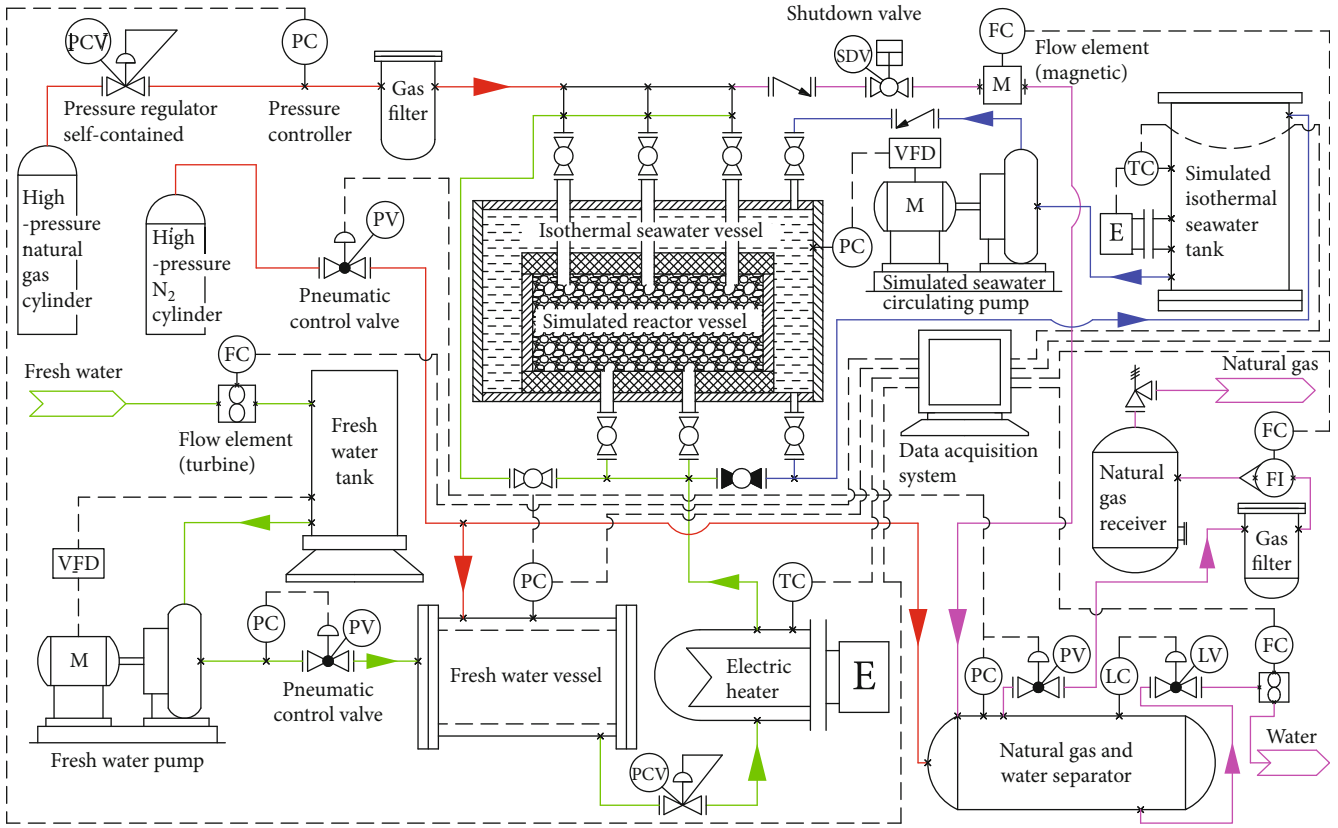

FIGURE 1: Process flow diagram of the offshore NGH formation and dissociation system by depressurization.

Figures 2 and 3 describe the variations of offshore natural gas flow rate and cumulative natural gas production with producing time in the 3-D marine sediments under depressurization. It can be seen from Figure 3 that the numerical results accord well with the experimental results of natural gas production. Based on the characteristics of gas flow in marine sediments, the offshore natural gas production process can be divided into three phases. During the prophase, the natural gas production increases rapidly. The large pressure gradient induced by pressure drawdown distribution at the bottom of the production well drives free natural gas flow into the wellbore. As a result, NGH is undergoing initially rapid dissociation, which produces a large amount of free natural gas. During the second phase, the natural gas production decreases slowly. The temperature of hydrate-bearing formation decreases in marine sediments, and heat conduction cannot transfer to the dissociation area, which causes insufficient energy supply for further NGH dissociation at a high rate. Free natural gas far from the production well cannot then flow into the wellbore because of the low pressure gradient, which would reduce the natural gas flow rate. During the final phase, the natural gas production is low. Most NGHs have dissociated and much sensible heat has been consumed in marine sediments. Temperature and pressure of the hydrate-bearing formation decrease and the dissociation of NGH is slowed down. The low pressure gradient aggravates the reduction of the natural gas flow rate. Therefore, the feasible technology of oceanic hydrate exploitation can utilize depressurization to dissociate NGH only during an initial phase. Afterwards, the production technology should switch to the combination of depressurization and thermal stimulation in order to compensate the deficiency in energy and the increase of ice saturation in marine sediments.

Comparison of cumulative natural gas production between the experimental and numerical results for the proposed methodology in 3-D marine sediments and the conventional methodology in 1-D marine sediments is shown in Figure 4.

The conventional methodology in 1-D marine sediments was developed to simulate the process of gas production from Berea sandstone samples containing methane hydrate by means of a depressurization mechanism. This methodology closely matched the experimental data of gas and water production, the progress of the dissociation front, the pressure and production, the progress of the dissociation front, and the pressure and saturation profiles. However, the conventional methodology in 1-D marine sediments does not perform well for offshore NGH dissociation in 3-D marine sediments. The main reason is that the mathematical models developed for 1-D natural gas production from the hydrate-bearing core by depressurization usually neglected the effect of NGH dissociation kinetics and the ice phase. Furthermore, the experimental results of 1-D marine sediments only

Table 1: The main experimental parameters and independent variables obtained for offshore NGH dissociation.

Physical variables	Values
Porosity Φ_0	0.305
The intrinsic permeability k (μm^2)	0.45
Initial saturation of NGH S_{mh}	0.63
Initial saturation of water S_w	0.21
Initial saturation of natural gas S_{ng}	0.68
Specific heat of ice h_I ($J{\cdot}kg^{-1}{\cdot}K^{-1}$)	2105
Specific heat of NGH h_{mh} ($J{\cdot}kg^{-1}{\cdot}K^{-1}$)	1795
Specific heat of marine sediment h_s ($J{\cdot}kg^{-1}{\cdot}K^{-1}$)	850
Specific heat of water h_w ($J{\cdot}kg^{-1}{\cdot}K^{-1}$)	4215
Thermal conductivity of ice C_I ($W{\cdot}K^{-1}{\cdot}m^{-1}$)	3.45
Thermal conductivity of NGH C_{mh} ($W{\cdot}K^{-1}{\cdot}m^{-1}$)	0.50
Thermal conductivity of natural gas C_{ng} ($W{\cdot}K^{-1}{\cdot}m^{-1}$)	0.07
Thermal conductivity of water C_w ($W{\cdot}K^{-1}{\cdot}m^{-1}$)	0.60
Initial temperature T_0 (K)	281.4
Temperature at the bottom of the wellbore T_{wf} (K)	281.4
Initial pressure p_0 (MPa)	5.82
Density of ice ρ_I ($kg{\cdot}m^{-3}$)	902
Density of NGH ρ_{mh} ($kg{\cdot}m^{-3}$)	910
Density of marine sediment ρ_s ($kg{\cdot}m^{-3}$)	2500
Density of water ρ_w ($kg{\cdot}m^{-3}$)	1010
Viscosity of natural gas μ_{ng} (mPa·s)	0.01
Viscosity of water μ_w (mPa·s)	1.0

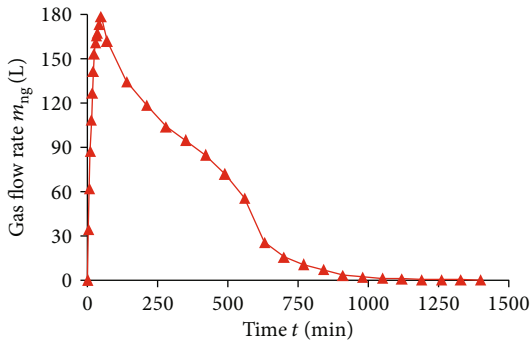

Figure 2: The variation of natural gas flow rate with time in 3-D marine sediments for the whole offshore natural gas production process.

consider NGH dissociation that occurred initially throughout the sample with the temperature maintained above the ice point.

Figures 5 and 6 show the variations of water flow rate and cumulative water production with time in the 3-D marine sediments under depressurization. The water production process can also be divided into three phases. During the prophase, the water flow rate, relatively low compared with natural gas flow rate, rises to its maximum value. Under a large pressure gradient induced by pressure drawdown distribution, the flow ability into the wellbore of natural gas is superior to water. And thus, natural gas flow is preceded by water flow into the production wellbore and natural gas occupies more continuous flow channels than water. Then, the natural

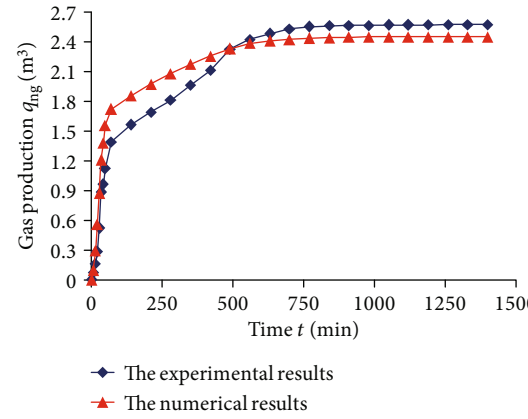

Figure 3: The variation of cumulative natural gas production with time in 3-D marine sediments for the whole offshore natural gas production process.

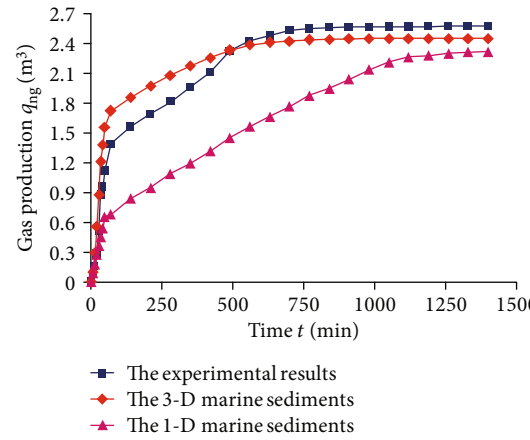

Figure 4: Comparison of cumulative natural gas production between the experimental and numerical results for the 3-D model and the conventional 1-D model in marine sediments.

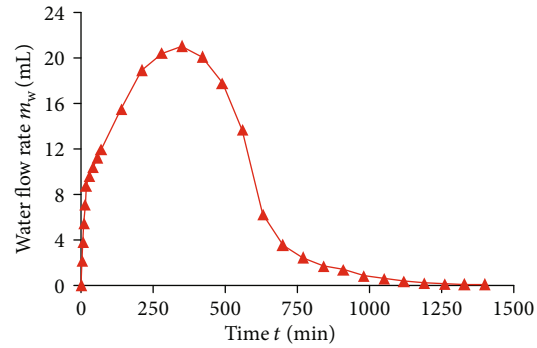

Figure 5: The variation of water flow rate with time in 3-D marine sediments for the whole water production process.

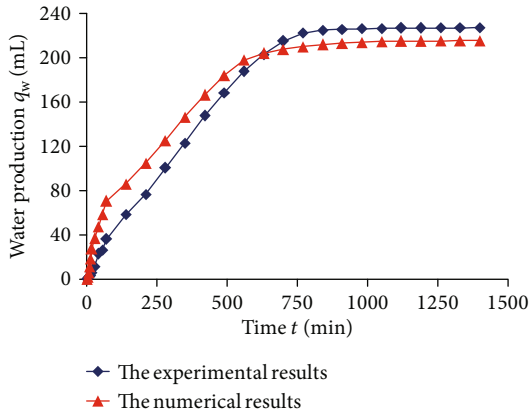

Figure 6: The variation of cumulative water production with time in 3-D marine sediments for the whole water production process.

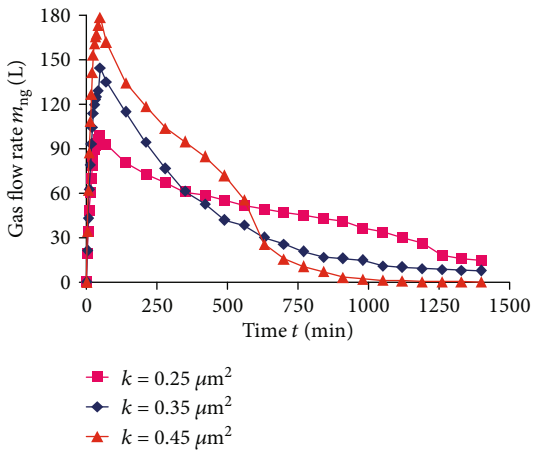

Figure 7: The effect of intrinsic permeability on offshore natural gas flow rate in 3-D marine sediments under depressurization.

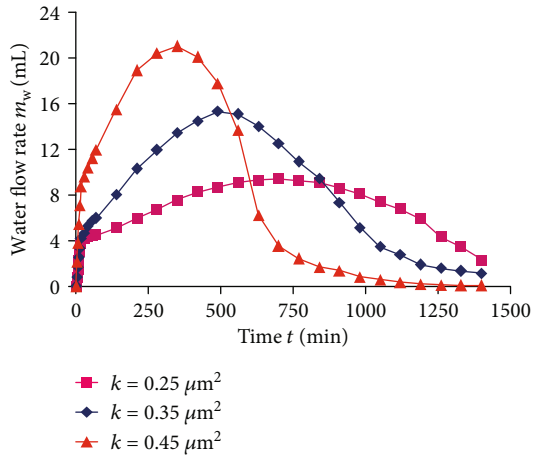

Figure 8: The effect of intrinsic permeability on water flow rate in 3-D marine sediments under depressurization.

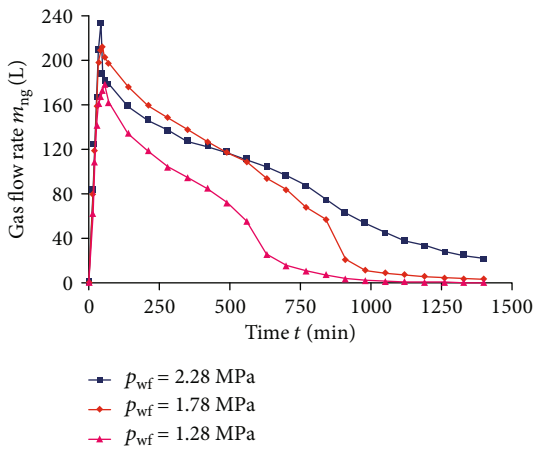

Figure 9: The effect of bottom-hole pressure of the production wellbore on offshore natural gas flow rate in 3-D marine sediments under depressurization.

gas flow rate begins to decline accompanied by an increase in water production. During the second phase, the water flow rate reaches the maximum value and then water production decreases. The production of water generated by NGH dissociation enhances with the depletion of pressure within the dissociation area. Then, water flow rate decreases due to the reduction of the amount of NGH dissociation. Furthermore, water freezing starts to occur in marine sediments, and more ice gradually forms with the depressurization. As a result, water production decreases rapidly during the final phase. Water generated by NGH dissociation is less, pressure gradient is low, and water freezes seriously in marine sediments. Therefore, pumping installations are needed for the offshore natural gas production process of oceanic hydrate exploitation under depressurization.

Figures 7 and 8 depict the relationships between offshore natural gas and water flow rates and the intrinsic permeability in the 3-D marine sediments under depressurization.

Offshore natural gas and water flow rates can be improved by an increase of the intrinsic permeability. But the stable period of natural gas production is even shorter under the conditions of high intrinsic permeability. More generally, the lower the intrinsic permeability in marine sediments, the later the water flow rate reaches the peak production. As a consequence, water production globally reduces with the intrinsic permeability. Therefore, the space interval of the production wellbore should be enlarged by the maximum intrinsic permeability. And drainage capacity of pumping water should be enhanced by an increase of the intrinsic permeability for oceanic hydrate exploitation under depressurization.

Figures 9 and 10 show the effects of bottom-hole pressure of the production wellbore on offshore natural gas and water flow rates in the 3-D marine sediments under depressurization. Natural gas flow rate does not increase with the decrease of bottom-hole pressure in production wellbores. The variation of natural gas flow rate with bottom-hole pressures of the production wellbore does not show a clear law. But the stable period of natural gas production is enhanced and the water flow rate is reduced with the increase of bottom-hole

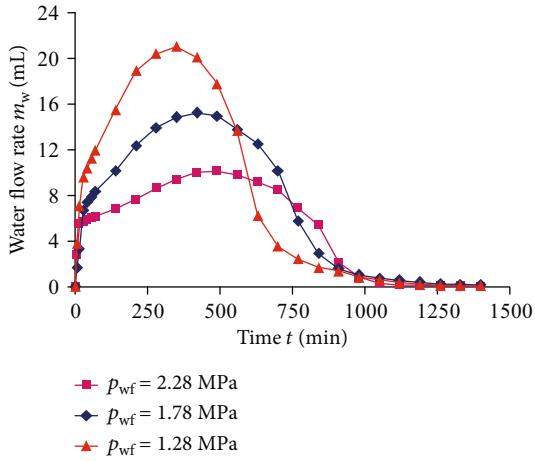

FIGURE 10: The effect of bottom-hole pressure of the production wellbore on the water flow rate in 3-D marine sediments under depressurization.

pressure in production wellbores. The main reason is that offshore NGHs dissociate slowly which gradually consumes the energy of marine sediments under the low producing pressure. Furthermore, the energy in sediments cannot transfer to the areas of NGH dissociation because of the restriction of heat conductivity under the conditions of low temperature. And this may cause the areas of NGH dissociation to become frozen and result in the blockage of pores in marine sediments and aggravates the reduction of natural gas flow rate. Therefore, the bottom-hole pressure in production wellbores should be adjusted reasonably according to the well conditions and the behavior of NGH reservoirs.

5. Conclusions

This work presents a methodology that involves a numerical integration technique to predict and analyze the dynamic characteristics of NGH dissociation under depressurization. This provides the theoretical basis to analyze technical issues of oceanic hydrate exploitation. It comes out that

(1) during the prophase, NGH is undergoing initially rapid dissociation and natural gas flow rate increases effectively thanks to the large pressure gradient induced by pressure drawdown distribution. During the second phase, natural gas flow rate decreases slowly because of the decreased temperature of hydrate-bearing formation and the low pressure gradient. During the final phase, natural gas flow rate is low because most NGHs have dissociated and much sensible heat has been consumed in marine sediments

(2) during the prophase, natural gas flow is preceded by water flow into the production wellbore and natural gas occupies more continuous flow channels than water under a large pressure gradient. Then, the natural gas flow rate begins to decline accompanied by an increase of water production. During the second phase, the water flow rate enhances with the depletion of pressure and then decreases with the reduced amount of NGH dissociation and the increased ice formation. During the final phase, water production decreases rapidly because water generated by NGH dissociation is less and water freezes seriously

(3) the stable period of natural gas production is even shorter under the conditions of high intrinsic permeability. The lower the intrinsic permeability in marine sediments, the later the water flow rate reaches the peak production. Water production globally reduces with the intrinsic permeability. And the space interval of the production wellbore should be enlarged by an increase of the intrinsic permeability

(4) the natural gas flow rate does not increase with the decrease of bottom-hole pressure. The stable period of natural gas production is enhanced, and the water flow rate reduces with the increase of bottom-hole pressure. The main reason is the slow offshore NGH dissociation under the low producing pressure and the restriction of heat conductivity under the conditions of low temperature. And this may result in water freeze and the blockage of pores in marine sediments and aggravates the reduction of natural gas flow rate

Data Availability

The data used to support the findings of this study are included within the article (Table 1).

Conflicts of Interest

No potential conflict of interest was reported by the authors.

Acknowledgments

This work was financially supported by the National Science and Technology Major Project of the Ministry of Science and Technology of China under Award No. 2016ZX05065-001, Key Research Project of Shandong Province under Award No. 2019GHY112029 and No. 2019GSF109090, and Higher Education Research and Development Project of Shandong Province under Award No. J17KA033.

References

[1] T. S. Collett, A. H. Johnson, C. C. Knapp, and R. Boswell, "Natural gas hydrates: a review," *Browse Collections*, vol. 89, no. 1, pp. 146–219, 2009.

[2] D. A. Wood, "Gas hydrate research advances steadily on multiple fronts: a collection of published research (2009–2015)," *Journal of Natural Gas Science and Engineering*, vol. 24, no. 5, pp. A1–A8, 2015.

[3] M. D. Max, A. H. Johnson, and W. P. Dillon, *Economic Geology of Natural Gas Hydrate*, Springer, Berlin, Dordrecht, 2006.

[4] J. H. van der Waals, "The statistical mechanics of clathrate compounds," *Transactions of the Faraday Society*, vol. 52, no. 0, pp. 184–193, 1956.

[5] W. Lin and G. J. Chen, "Review of research on the dissociation kinetics of gas hydrate," *Chinese Journal of Process Engineering*, vol. 4, no. 1, pp. 69–74, 2004.

[6] E. Dendy Sloan Jr., C. A. Koh, and C. A. Koh, *Clathrate Hydrates of Natural Gases*, CRC Press, Boca Raton, FL, USA, 3rd edition, 2007.

[7] M. S. Selim and E. D. Sloan, "Heat and mass transfer during the dissociation of hydrates in porous media," *AIChE Journal*, vol. 35, no. 6, pp. 1049–1052, 1989.

[8] M. Clarke and P. R. Bishnoi, "Determination of the intrinsic rate of ethane gas hydrate decomposition," *Chemical Engineering Science*, vol. 55, no. 21, pp. 4869–4883, 2000.

[9] M. Clarke and P. R. Bishnoi, "Determination of the activation energy and intrinsic rate constant of methane gas hydrate decomposition," *The Canadian Journal of Chemical Engineering*, vol. 79, no. 1, pp. 143–147, 2001.

[10] M. A. Clarke and P. R. Bishnoi, "Determination of the intrinsic kinetics of CO_2 gas hydrate formation using in situ particle size analysis," *Chemical Engineering Science*, vol. 60, no. 3, pp. 695–709, 2005.

[11] X. X. He, J. S. Yu, Y. H. Ma, S. Zhang, and F. Liu, "Particle shrinking dynamic model for methane hydrate decomposition," *Natural Gas Geoscience*, vol. 16, no. 6, pp. 818–821, 2005.

[12] G. Ahmadi, C. Ji, and D. H. Smith, "Numerical solution for natural gas production from methane hydrate dissociation," *Journal of Petroleum Science and Engineering*, vol. 41, no. 4, pp. 269–285, 2004.

[13] C. Ji, G. Ahmadi, and D. H. Smith, "Constant rate natural gas production from a well in a hydrate reservoir," *Energy Conversion and Management*, vol. 44, no. 15, pp. 2403–2423, 2003.

[14] G. G. Tsypkin, "Regimes of dissociation of gas hydrates coexisting with a gas in natural strata," *Journal of Engineering Physics and Thermophysics*, vol. 74, no. 5, pp. 1083–1089, 2001.

[15] G. J. Moridis, "Numerical studies of gas production from methane hydrates," *SPE Journal*, vol. 8, no. 4, pp. 359–370, 2003.

[16] L. Chen, H. Yamada, Y. Kanda et al., "Numerical analysis of core-scale methane hydrate dissociation dynamics and multiphase flow in porous media," *Chemical Engineering Science*, vol. 153, no. 10, pp. 221–235, 2016.

[17] S. Li, X. Xu, R. Zheng, Y. Chen, and J. Hou, "Experimental investigation on dissociation driving force of methane hydrate in porous media," *Fuel*, vol. 160, no. 11, pp. 117–122, 2015.

[18] X. S. Li, C. G. Xu, Y. Zhang, X. K. Ruan, G. Li, and Y. Wang, "Investigation into gas production from natural gas hydrate: a review," *Applied Energy*, vol. 172, no. 6, pp. 286–322, 2016.

[19] L. Ruffine, "Exploring methane-hydrate formation and dissociation in geologic materials through laboratory experiments: kinetic behavior and morphology," *Fuel*, vol. 141, no. 5, pp. 173–184, 2015.

[20] Z. Yin, Z. R. Chong, H. K. Tan, and P. Linga, "Review of gas hydrate dissociation kinetic models for energy recovery," *Journal of Natural Gas Science and Engineering*, vol. 35, Part B, pp. 1362–1387, 2016.

[21] J. Boxall, G. David, J. Mulligan, C. Koh, and E. D. Sloan, "Gas hydrate formation and dissociation from water-in-oil emulsions studied using PVM and FBRM particle size analysis," in *6th International Conference on Gas Hydrates*, pp. 1–9, Vancouver, Canada, July 2008.

[22] H. P. Veluswamy, Q. W. Hong, and P. Linga, "Morphology study of methane hydrate formation and dissociation in the presence of amino acid," *Crystal Growth & Design*, vol. 16, no. 10, pp. 5932–5945, 2016.

[23] C. S. Xiang, B. Z. Peng, H. Liu, C. Y. Sun, G. J. Chen, and B. J. Sun, "Hydrate formation/dissociation in (natural gas + water + diesel oil) emulsion systems," *Energies*, vol. 6, no. 2, pp. 1009–1022, 2013.

[24] Q. G. Meng, C. L. Liu, Y. G. Ye, and G. W. Hu, "Experimental research on dissociation kinetics of different gas hydrates," *Geoscience*, vol. 24, no. 3, pp. 607–613, 2010.

[25] V. E. Nakoryakov and S. Y. Misyura, "Kinetics of methane hydrate dissociation," *Doklady Physical Chemistry*, vol. 464, no. 2, article 9422, pp. 244–246, 2015.

[26] G. G. Tsypkin, "Formation of the impermeable layer in the process of methane hydrate dissociation in porous media," *Fluid Dynamics*, vol. 52, no. 5, pp. 657–665, 2017.

[27] X. Sun and K. K. Mohanty, "Kinetic simulation of methane hydrate formation and dissociation in porous media," *Chemical Engineering Science*, vol. 61, no. 11, pp. 3476–3495, 2006.

[28] M. Liang, G. Chen, C. Sun, L. Yan, J. Liu, and Q. Ma, "Experimental and modeling study on decomposition kinetics of methane hydrates in different media," *The Journal of Physical Chemistry B*, vol. 109, no. 40, pp. 19034–19041, 2005.

[29] A. Kumar, O. S. Kushwaha, P. Rangsunvigit, P. Linga, and R. Kumar, "Effect of additives on formation and decomposition kinetics of methane clathrate hydrates: application in energy storage and transportation," *The Canadian Journal of Chemical Engineering*, vol. 94, no. 11, pp. 2160–2167, 2016.

[30] L. G. Tang, X. S. Li, Z. P. Feng, G. Li, and S. S. Fan, "Control mechanisms for gas hydrate production by depressurization in different scale hydrate reservoirs," *Energy & Fuels*, vol. 21, no. 1, pp. 227–233, 2007.

[31] K. Nazridoust and G. Ahmadi, "Computational modeling of methane hydrate dissociation in a sandstone core," *Chemical Engineering Science*, vol. 62, no. 22, pp. 6155–6177, 2007.

[32] T. J. Kneafsey and G. J. Moridis, "Methane hydrate dissociation by depressurization in a Mount Elbert sandstone sample: experimental observations and numerical simulations," in *OTC Arctic Technology Conference*, pp. 150–161, Houston, TX, USA, February 2011.

[33] Z. J. Ai and J. Wang, "Study on kinetic model of natural gas hydrate dissociation," *Natural Gas Geoscience*, vol. 28, no. 3, pp. 377–382, 2017.

[34] C. Windmeier and L. R. Oellrich, "Theoretical study of gas hydrate decomposition kinetics: model predictions," *The Journal of Physical Chemistry A*, vol. 117, no. 47, pp. 12184–12195, 2013.

[35] C. Windmeier and L. R. Oellrich, "Experimental study of methane hydrate decomposition kinetics," *Chemie Ingenieur Technik*, vol. 87, no. 7, pp. 910–921, 2015.

[36] J. Chen, J. Liu, G. Q. Chen, C. Y. Sun, M. L. Jia, and B. Liu, "Insights into methane hydrate formation, agglomeration, and dissociation in water + diesel oil dispersed system," *Energy Conversion and Management*, vol. 86, no. 10, pp. 886–891, 2014.

[37] B. H. Shi, S. F. Song, X. F. Lv et al., "Investigation on natural gas hydrate dissociation from a slurry to a water-in-oil

emulsion in a high-pressure flow loop," *Fuel*, vol. 233, no. 12, pp. 743–758, 2018.

[38] S. Kimoto, F. Oka, and T. Fushita, "A chemo–thermo–mechanically coupled analysis of ground deformation induced by gas hydrate dissociation," *International Journal of Mechanical Sciences*, vol. 52, no. 2, pp. 365–376, 2010.

[39] S. Kimoto, H. Iwai, T. Akaki, and F. Oka, "Instability of dissociation process of methane hydrate bearing soil," in *Bifurcation and Degradation of Geomaterials in the New Millennium*, pp. 245–251, Springer, Cham, Switzerland, 2014.

[40] F. Oka, T. Adachi, and A. Yashima, "A strain localization analysis using a viscoplastic softening model for clay," *International Journal of Plasticity*, vol. 11, no. 5, pp. 523–545, 1995.

[41] R. Ashena and J. Moghadasi, "Bottom hole pressure estimation using evolved neural networks by real coded ant colony optimization and genetic algorithm," *Journal of Petroleum Science and Engineering*, vol. 77, no. 3-4, pp. 375–385, 2011.

[42] M. Liu, B. Bai, and X. Li, "A unified formula for determination of wellhead pressure and bottom-hole pressure," *Energy Procedia*, vol. 37, pp. 3291–3298, 2013.

[43] X. F. Liu, C. H. Liu, and Y. G. Qi, "Operating performance of sucker rod pump for the pumping system in coalbed methane wells," *Journal of Mechanical Engineering*, vol. 53, no. 8, pp. 195–200, 2017.

[44] X. F. Liu, C. H. Liu, and J. J. Wu, "A modern approach to analyzing the flowing pressures of a two-phase CBM and water column in producing wellbores," *Geofluids*, vol. 2019, Article ID 3093707, 9 pages, 2019.

[45] X. F. Liu, C. H. Liu, J. J. Wu, and Y. G. Qi, "Migration models of pulverized coal flowing with fluid and its production in CBM channels for the coal reservoirs," *Journal of China Coal Society*, vol. 43, no. 3, pp. 770–775, 2018.

[46] C. A. Mora and R. A. Wattenbarger, "Analysis and verification of dual porosity and CBM shape factors," *Journal of Canadian Petroleum Technology*, vol. 48, no. 2, pp. 17–21, 2009.

[47] R. P. Sutton, "An accurate method for determining oil PVT properties using the standing-Katz gas Z-factor chart," *SPE Reservoir Evaluation & Engineering*, vol. 11, no. 2, pp. 246–266, 2008.

[48] H. C. Kim, P. R. Bishnoi, R. A. Heidemann, and S. S. H. Rizvi, "Kinetics of methane hydrate decomposition," *Chemical Engineering Science*, vol. 42, no. 7, pp. 1645–1653, 1987.

[49] P. Mekala, P. Babu, J. S. Sangwai, and P. Linga, "Formation and dissociation kinetics of methane hydrates in seawater and silica sand," *Energy & Fuels*, vol. 28, no. 4, pp. 2708–2716, 2014.

[50] A. A. Amooey, "A novel correlational approach to estimating natural gas viscosity," *Journal of Engineering Physics and Thermophysics*, vol. 88, no. 3, pp. 769–773, 2015.

[51] T. Ertkin, J. H. Abou-Kassem, and G. R. King, *Basic Applied Reservoir Simulation*, Society of Petroleum Engineerings, Richardson, TX, USA, 2001.

[52] X. Sun, N. Nanchary, and K. K. Mohanty, "1-D modeling of hydrate depressurization in porous media," *Transport in Porous Media*, vol. 58, no. 3, pp. 315–338, 2005.

[53] T. Ahn, J. Lee, D. G. Huh, and J. M. Kang, "Experimental study on two-phase flow in artificial hydrate-bearing sediments," *Geosystem Engineering*, vol. 8, no. 4, pp. 101–104, 2005.

[54] M. D. Max and A. H. Johnson, *Exploration and Production of Oceanic Natural Gas Hydrate*, Springer, Cham, Switzerland, 2016.

[55] Y. Bie, M. Li, R. Malekian, F. Chen, Z. Feng, and Z. Li, "Effect of phase transition temperature and thermal conductivity on the performance of latent heat storage system," *Applied Thermal Engineering*, vol. 135, no. 5, pp. 218–227, 2018.

[56] V. P. Trubitsyn, A. N. Evseev, A. A. Baranov, and A. P. Trubitsyn, "Convection in the mantle with an endothermic phase transition," *Izvestiya, Physics of the Solid Earth*, vol. 43, no. 12, article 12001, pp. 981–991, 2007.